ORC Waste Heat Recovery System for the Turboshaft Engines of Turboelectric Aircraft correction

Krempus, D.; Beltrame, F.; Majer, M.; Colonna, Piero; de Servi, C.M.; Vos, Roelof

Publication date
2024

Note: The work documented in this report was presented at Aerospace Europe Conference 2023 - 10^{TH} EUCASS - 9^{TH} CEAS and published with the doi: 10.13009/EUCASS2023-658. This report corrects an error identified in the original publication related to the code used to produce the results of the CC-TS aircraft. The error resulted in an overprediction of the free power turbine isentropic efficiency of the CC-TS engine concept by approximately 2 absolute percent points. As a result the fuel savings obtained by employing the CC-TS engine concept as documented in the original publication are too high.

ORC Waste Heat Recovery System for the Turboshaft Engines of Turboelectric Aircraft

Dabo Krempus[⋆†] *Fabio Beltrame*[⋆], *Matteo Majer*[⋆],
Carlo Maria De Servi[⋆§], Roelof Vos[⋆⋆] and Piero Colonna[⋆]
[⋆]*Propulsion and Power, Delft University of Technology, The Netherlands*
[⋆⋆]*Flight Performance and Propulsion, Delft University of Technology, The Netherlands*
[§] *VITO, Thermal Energy Systems, Mol, Belgium*
[†]Corresponding author, d.krempus@tudelft.nl

ABSTRACT

This paper presents a preliminary study about a combined-cycle engine based on a turboshaft engine and an organic-Rankine-cycle (ORC) bottoming unit to be used onboard an aircraft with a turboelectric propulsion system. The aim is to analyse whether benefits with respect to mission fuel consumption can be derived by employing such a combined-cycle engine when compared to a simple-cycle turboshaft engine. For this purpose, a multidisciplinary optimization framework is developed, incorporating models for the engine, ORC system, ORC turbine, heat exchangers, and mission analysis. This framework is coupled with an optimizer to identify the optimal combined-cycle engine design for minimum mission fuel consumption. The results suggest that fuel savings of around 1.5% are possible with the optimized system if compared to the aircraft employing turboshaft engines. Heat exchanger volume is identified as the most constraining parameter when it comes to combined-cycle performance. The analysis of the results suggests as aspects which might lead to further improvements the evaluation of other ORC architectures, working fluids and heat exchanger topologies.

1. INTRODUCTION

The thermal efficiency of modern aero-engines is around 50%. This means that half of the chemical energy provided by the combustion of fossil fuel is lost to the environment in the form of a hot exhaust gas stream. Improvements in thermal efficiency of conventional gas turbines can be achieved with increasing turbine inlet temperature (TIT) and overall pressure ratio (OPR). However, further efficiency improvements by these means proof increasingly difficult due to material limitations and emission regulations [31]. Modifications to the thermodynamic cycle may allow to overcome this limitation. Various ideas such as architectures employing recuperation and/or intercooling as well as combined cycle configurations have been studied in the past [5, 49, 38]. However, such cycle configurations, which are standard in the power sector, have not been realized yet as aircraft propulsion systems. Organic-Rankine-cycle (ORC) bottoming units for medium-power capacity stationary gas turbines have been successfully deployed [27]. ORC waste-heat-recovery (WHR) systems are also employed on board of vessels and have been thoroughly tested as a way of improving the fuel efficiency of long-haul truck engines [27]. Only few recent studies analysed the effect of recovering otherwise wasted thermal energy with an ORC system from turbofan engines [37], turboprop engines [50] and reciprocating engines for general aviation aircraft [20]. These studies indicate a different level of possible fuel savings when employing such combined-cycle engines if compared to their simple-cycle counterparts, ranging from 1% to 15%. However, the research work conducted so far does differ in the level of modelling fidelity and only partially considers component sizing and airframe integration.

The preliminary research presented here aims at investigating ORC WHR systems onboard aircraft by means of more realistic, therefore more complex simulations and design optimization methods. Part of this effort is thus devoted to the development of a novel multidisciplinary simulation framework. This framework is coded in Python and includes modules for gas turbine and ORC performance simulations, ORC turbine and heat exchanger preliminary design as well as aircraft design and aircraft performance simulation. In an earlier work, this framework was employed to study a simple application scenario involving an aircraft auxiliary power unit whose performance is enhanced with an ORC WHR system to provide power on ground only [29]. The results indicate that fuel savings are possible, give a first insight into system design requirements, and highlight the importance of taking into account size limitations. This work

is about the adoption of a combined-cycle turboshaft engine (CC-TS) consisting of a turboshaft engine and an ORC WHR unit onboard a single-aisle turboelectric aircraft. The main research question is: What is the impact on mission fuel consumption of adopting an ORC WHR unit for turboshaft engines of a turboelectric aircraft? For this purpose an optimized CC-TS preliminary design is identified as a result of the minimization of mission fuel consumption taking into account size limitations.

The reference aircraft selected for this study is the ONERA Dragon turboelectric aircraft concept [43]. This aircraft employs two turboshaft engines housed in pods in the aft of the aircraft to provide electrical power to an under-the-wing distributed propulsion system consisting of electrically-driven ducted fans. Research indicates that aerodynamic benefits of this configuration can improve fuel consumption by 7% compared to a traditional tube-and-wing aircraft employing turbofan engines with the same technology level of turboshaft engines that is assumed to be a year 2035 entry into service [43]. The work at hand analyses the performance of this aircraft architecture when replacing the turboshaft engines with CC-TS engines and is referred to as Dragon CC-TS.

Figure 1: Rendering of the ONERA Dragon aircraft concept as presented in Ref. [43].

Table 1: Top level aircraft requirements (TLARs) of the ONERA Dragon [43]

Parameter	Input
Range (nmi/km)	2750/5100
Number of passengers (-)	150
Mach number (-)	0.78
Design payload (kg)	13600

2. METHODOLOGY

The numerical framework developed for the preliminary design and evaluation of the CC-TS system is modular and all modules are integrated into a system model using the Python library *openMDAO* [16]. The framework is hereafter referred to as the ARENA framework and the acronym ARENA stands for airborne energy harvesting for aircraft. Figure 2 shows the extended design structure matrix (XDSM) of the system model containing all its major modules. Figure 3 shows the process flow diagram (PFD) of the CC-TS.

2.1 Optimization Problem

Numerical optimization is used to identify a CC-TS design that minimizes mission fuel mass (m_{fuel}). Therefore, the following single-objective optimization problem is solved:

$$\begin{aligned} \text{minimize} \quad & F(x) = m_{\text{fuel}}(x) \\ \text{subject to:} \quad & x_{\text{i}}^{L} \leq x_{\text{i}} \leq x_{\text{i}}^{U} \end{aligned} \tag{1}$$

The design vector (x) is composed of 18 variables which relate to the thermodynamic cycle and the preliminary design of the components of the CC-TS system, namely the turboshaft engine, the ORC, the heat exchangers, the ORC turbogenerator and the ram-air duct. Table 2 lists the design variables x_{i} considered in the optimization together with their lower bounds (x_{i}^{L}) and upper bounds (x_{i}^{U}). The optimization problem is solved using a genetic algorithm implemented in the Python library *pymoo* [4]. A population size of approximately ten times the number of design variables is used for the genetic algorithm. The convergence criterion is that the relative change between the last and the 5$^{\text{th}}$ to last generation is below 10^{-6}.

2.2 Aircraft Aerodynamics, Mass and Performance

This module of the ARENA framework performs aircraft mass and mission analysis. This process includes the evaluation of: 1) lift coefficient (C_{L}) and drag coefficient (C_{D}), 2) maximum take-off mass (m_{mto}), 3) mission fuel mass (m_{fuel}), 4) required generator output power during take-off ($\dot{W}_{\text{to}}$) and wing area (S_{ref}), 5) cruise altitude (h_{cr}) and 6) required generator output power during cruise ($\dot{W}_{\text{cr}}$).

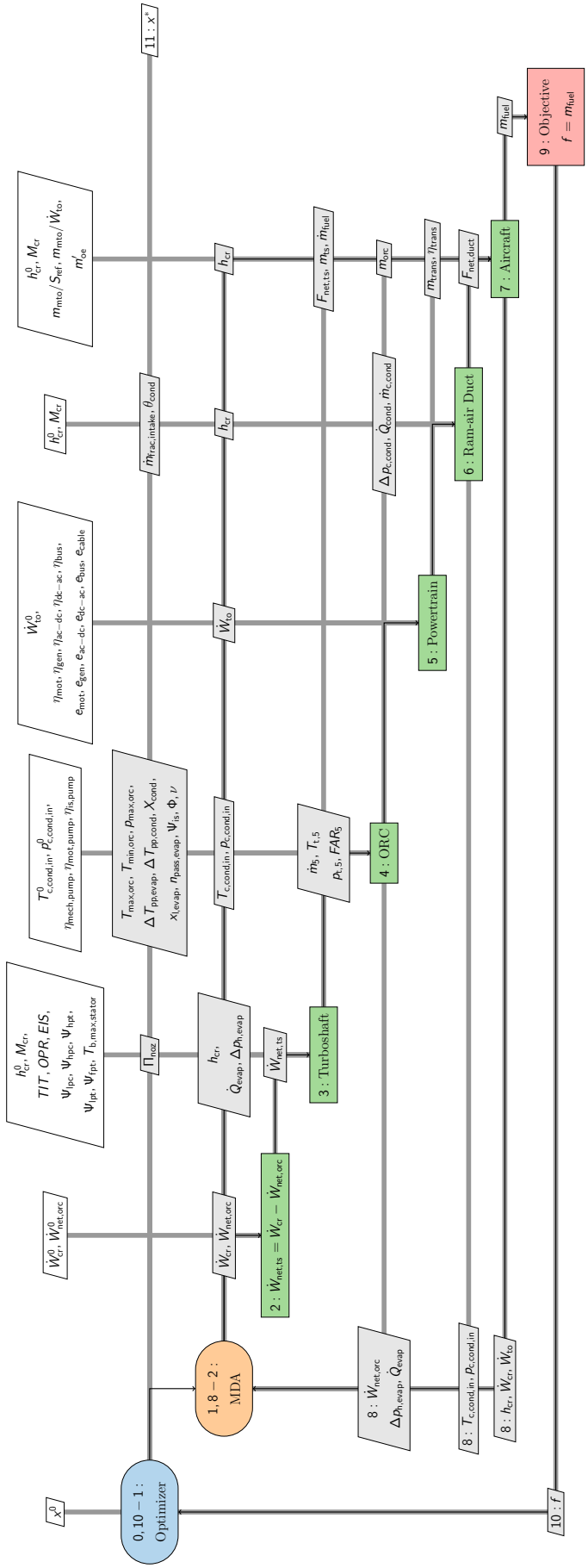

Figure 2: XDSM of the Dragon CC-TS system model.

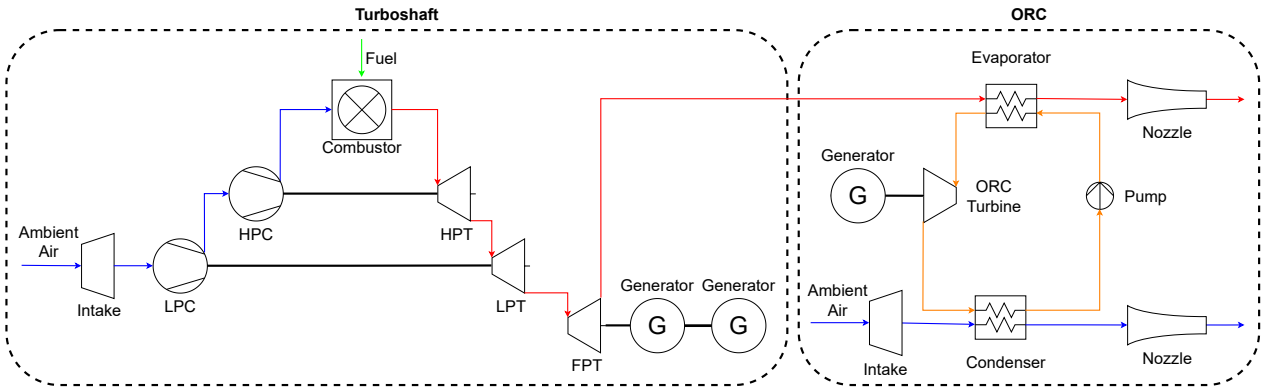

Figure 3: Process flow diagram of the CC-TS configuration.

Table 2: CC-TS design variables and their corresponding bounds.

Model	Variables (x_i)	Description (Unit)	Bounds (x^L/x^U)
Turboshaft	Π_{noz}	Nozzle pressure ratio (-)	1.05/1.4
ORC	$T_{min,orc}$	Minimum cycle temperature (K)	323/423
	$T_{max,orc}$	Maximum cycle temperature (K)	520/570
	$p_{max,orc}$	Maximum cycle pressure (Pa)	$1.1p_{crit}$/$1.5p_{crit}$
	$\Delta T_{pp,cond}$	Condenser pinch point temperature difference (K)	20/100
	$\Delta T_{pp,evap}$	Evaporator pinch point temperature difference (K)	20/100
ORC HEX	X_{cond}	Condenser flat-tube length (m)	0.5/1.0
	$\phi_{l,cond}$	Condenser louver angle (deg)	10/30
	$b_{f,cond}$	Condenser fin height (mm)	7.0/12.0
	$p_{f,cond}$	Condenser fin pitch (mm)	1.0/4.0
	$x_{t,evap}$	Evaporator non-dimensional transversal pitch (-)	1.25/3.00
	$x_{l,evap}$	Evaporator non-dimensional longitudinal pitch (-)	1.25/3.0
	$n_{pass,evap}$	Evaporator number of passes (-)	8/19
Ram-air Duct	$\dot{m}_{frac,intake}$	Intake design mass flow rate ratio (-)	0.4/1.0
	θ_{cond}	Condenser tilt angle (°)	45/75
ORC Turbo Generator	ψ_{is}	Isentropic stage loading (-)	0.4/1.3
	ϕ	Flow coefficient (-)	0.10/0.40
	ν	Hub-to-tip ratio (-)	0.40/0.65

A three-term drag polar of the aircraft in the form $C_D = C_{D,min} + K_L(C_L - C_{L,min})^2$ [47] is adopted. The coefficient $C_{D,min}$ is approximated to be equal to the zero-lift drag coefficient of the two-term drag polar and approximated based on the method of Obert [36]. The coefficients K_L and $C_{L,min}$ are determined based on estimated cruise lift and drag coefficients of the ONERA Dragon. The resulting coefficients are $C_{D,min} = 0.0183$, $K_L = 0.0937$ and $C_{L,min} = 0.160$. In the case of the Dragon CC-TS, the net force arising from the ram-air duct is interpreted as a change in zero-lift drag and results in a parallel shift of the drag polar.

Mass estimation of turboelectric and hybrid-electric aircraft architectures poses a challenge to conceptual aircraft design as commonly used empirical laws relating m_{mto} to operating empty mass (m_{oe}) do not cover these novel configurations. It is therefore necessary to apply a more detailed component based mass estimation method. In this work a method proposed by De Vries et al. [10] is used. This method assumes that m_{oe} minus wing mass (m_{wing}) and powertrain mass (m_{pt}), hereafter referred to as m'_{oe}, is independent of the powertrain architecture. m_{oe} can subsequently be determined as

$$m_{oe} = m'_{oe} + m_{pt} + m_{wing}. \tag{2}$$

m'_{oe} can either be calculated by further subdivinding the airframe into its major components and applying empirical relations to determine the corresponding masses, or in case of a retrofitting scenario it might be possible to derive its value for the reference aircraft. m'_{oe} is approximated to be 24 900 kg for the ONERA Dragon. There are no empirical

methods available to estimate the wing mass of aircraft employing a distributed wing-mounted propulsion system. In this work the method of Torenbeek [45, App. C] is applied; it provides good sensitivity of the wing mass to major design parameters including the option to consider 0, 2 or 4 wing-mounted engines. The wing mass estimated with this method assuming 4 wing-mounted engines shows good agreement with the wing mass estimated for the ONERA Dragon (see Tab. 5), if geometrical details of the wing such as thickness-to-chord ratio, inclination angles, wing sweep and wing aspect ratio are set to the values provided by Schmollgruber et al. [43].

Mission fuel mass is estimated based on the Breguet range equation for cruise-climb in combination with a definition of an equivalent cruise range according to Torenbeek [46]. This equivalent cruise range includes the nominal cruise range according to the top level aircraft requirements (TLARs), a lost range representing the amount of fuel required for climbing and the range required for divergence, holding and contingency. A divergence range of 400 km, a holding time of 30 min and a contingency fraction of 5% are assumed. Cruise is performed at constant Mach number and at maximum lift-to-drag ratio (L/D) resulting in a continuous cruise-climb trajectory.

To ensure that the Dragon CC-TS fulfills the design requirements of the ONERA Dragon aircraft, the same wing loading and power loading at maximum take-off mass is adopted. Using these values together with the evaluated m_{mto}, the values of $\dot{W}_{\mathrm{to}}$ and S_{ref} are determined. Note that $\dot{W}_{\mathrm{cr}}$ and $\dot{W}_{\mathrm{to}}$ refer to generator output power.

In the second to last step, the h_{cr} is determined based on the given Mach number, C_{L} and mid-cruise aircraft mass. In the last step, the required generator output power during cruise is evaluated taking into account the residual jet thrust ($F_{\mathrm{net,ts}}$) produced by the CC-TS engines according to the power balance

$$\dot{W}_{\mathrm{cr}} = \frac{(D - 2F_{\mathrm{net,ts}})v_{\infty}}{\eta_{\mathrm{trans}}\eta_{\mathrm{prop}}}, \tag{3}$$

where D is the aircraft drag, v_{∞} the cruise velocity, η_{trans} the electrical powertrain efficiency (see Section 2.3) and η_{prop} the propulsive efficiency. All cruise-related parameters are evaluated based on the mid-cruise aircraft mass (m_{cr}) approximated according to [46] as $m_{\mathrm{cr}} = \sqrt{m_{\mathrm{mto}}(m_{\mathrm{mto}} - m_{\mathrm{fuel,cr}})}$, where $m_{\mathrm{fuel,cr}}$ is the fuel mass required for the cruise range according to the TLARs.

2.3 Powertrain

The powertrain architecture of the Dragon CC-TS is the same as that of the ONERA Dragon with the exception of the added ORC unit. The main components of the powertrain are the CC-TS, electrical power transmission components and ducted-fans. The distributed propulsion system consists of 26 ducted fans. Figure 4 shows half of the cross-redundant architecture. Note that fault current limiters and circuit breakers are omitted in this figure for simplicity. Table 3 gives mass specific power and efficiency values of the electrical components, which are sized for maximum power demand, thus during take-off. Note that the indicated values for generator mass-specific power and efficiency do not apply to the ORC turbogenerator, and are determined by a separate preliminary design tool explained in Section 2.6.

The powertrain mass (m_{pt}) is the sum of two times the CC-TS mass (m_{ccts}) and the mass of the electrical power transmission components (m_{trans}). m_{ccts} is the sum of the turboshaft mass (m_{ts}), the mass of the two turboshaft mounted generators (m_{gen}), and the mass of the ORC unit assembly (m_{orc}). m_{trans} is the sum of the individual electrical component masses. These masses are determined by dividing rated power of each component by its mass-specific power value listed in Tab. 3. The variation of ducted-fan size and mass with input power and the variation of cooling system mass with rated power of the electrical components are not modelled. The masses of these components are considered fixed and included in the mass m'_{oe} (see Section 2.2).

The powertrain efficiency (η_{pt}) is defined as the product of the net CC-TS efficiency ($\eta_{\mathrm{net,ccts}}$), the electrical component transmission efficiency (η_{trans}) and the ducted-fan propulsive efficiency (η_{prop}). The net efficiencies of the turboshaft, ORC system and CC-TS are defined as

$$\eta_{\mathrm{net,ts}} = \frac{\dot{W}_{\mathrm{net,ts}}}{\dot{m}_{\mathrm{fuel}} \cdot \mathrm{LHV}}, \eta_{\mathrm{net,orc}} = \frac{\dot{W}_{\mathrm{net,orc}}}{\dot{Q}_{\mathrm{evap}}}, \eta_{\mathrm{net,ccts}} = \frac{\dot{W}_{\mathrm{net,ccts}}}{\dot{m}_{\mathrm{fuel}} \cdot \mathrm{LHV}}, \tag{4}$$

where $\dot{m}_{\mathrm{fuel}}$ is the fuel mass flow rate, $\dot{Q}_{\mathrm{evap}}$ the thermal power recovered by the evaporator and LHV the lower heating value of the fuel which is 43 MJ/kg. The CC-TS net power output ($\dot{W}_{\mathrm{net,ccts}}$) is the sum of turboshaft net power output ($\dot{W}_{\mathrm{net,ts}}$) and ORC net power output ($\dot{W}_{\mathrm{net,orc}}$). $\dot{W}_{\mathrm{net,ccts}}$ of a single CC-TS unit is half the required power demand during cruise $\dot{W}_{\mathrm{cr}}$ (Eq. 3) and take-off $\dot{W}_{\mathrm{to}}$, respectively. Note that net power output refers to generator power output of the turboshaft and ORC unit, also see Fig. 4. η_{trans} accounts for losses occurring in the electrical components between the CC-TS and the ducted-fans and is calculated as $\eta_{\mathrm{trans}} = \eta_{\mathrm{acdc}}\eta_{\mathrm{pmu}}\eta_{\mathrm{dcac}}\eta_{\mathrm{mot}}$, where η_{acdc} is the inverter efficiency, η_{pmu} the combined efficiency of the DC busses, η_{dcac} is the converter efficiency and η_{mot} the electrical motor efficiency. η_{prop} is set to 86%, which is the value applied for the ONERA Dragon [11].

The power specific fuel consumption (PSFC) is defined as the fuel mass flow rate divided by the total generator power output. The use of the generator power output instead of the engine shaft power output allows a direct comparison between aircraft configurations using simple-cycle turboshaft engines and CC-TS engines. The PSFC of CC-TS is calculated as

$$\mathrm{PSFC}_{\mathrm{ccts}} = \frac{\dot{m}_{\mathrm{fuel}}}{\dot{W}_{\mathrm{net,ccts}}}. \tag{5}$$

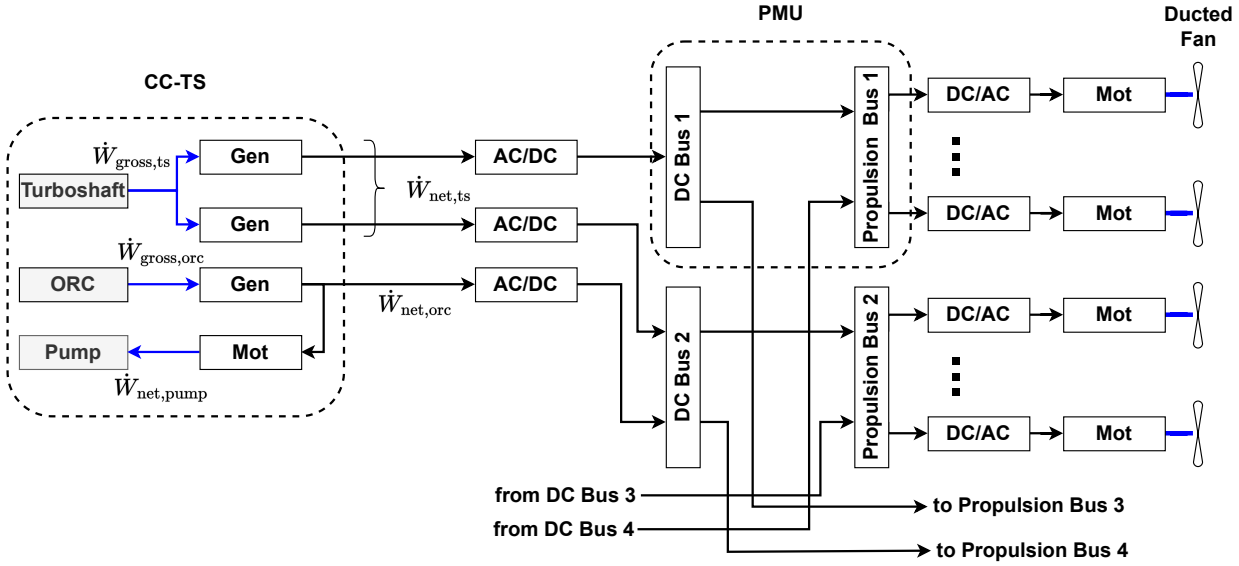

Figure 4: Dragon CC-TS powertrain architecture (adapted from Schmollgruber et al. [43]). Thick blue lines indicate mechanical power transmission, thick black lines electrical power transmission.

Table 3: Assumptions regarding the technology level of electric components. A moderate technology level is selected in accordance with the values provided in Ref. [43]

Component	**Mass specific power (kW/kg)**	**Efficiency (η)**
Generator (Gen)	13.5	0.95
Motor (Mot)	19.0	0.98
Inverter (AC/DC)	19.0	0.98
Converter (DC/AC)	19.0	0.98
Power management unit (PMU)	20.0	0.99
Cables	16.0*	1.00**

* The value is estimated by dividing the take-off power by the overall cable mass as given for the ONERA Dragon aircraft in Ref. [39] and is therefore not a generally applicable value.

** Cable losses are omitted for simplicity.

2.4 Engine

The turboshaft engine considered in this work is a two-spool engine with a free power turbine (FPT). The FPT powers to two electric generators. The use of two generators instead of one provides redundancy and their diameter is smaller than that of a single generator which is important for the integration with the turboshaft engine. The PFD of this engine is depicted on the left-hand side of Fig. 3. As show in the XDSM in Fig. 2 the turboshaft sub-model provides as output the performance of the turboshaft engine at design point.

2.4.1 Thermodynamic Modelling and Mass Estimation

The thermodynamic performance of the engine is calculated with the Python library *pycycle* [19]. Jet-A/A1 is used as the fuel. Turbomachinery polytropic efficiencies are determined using correlations presented by Samuelsson et al. [40], which are derived from the method described in [18, Ch. 5]. Based on statistical data, this method provides an estimate of turbomachinery efficiency as a function of the entry into service (EIS) year, and of the stage loading. It also takes into account scale effects based on the reduced mass flow rate ($\dot{m}_{\mathrm{red}}$). Furthermore, the method accounts for different turbomachinery types (axial/radial) and distinguishes between the turbomachinery of the low and high pressure sections of the engine. In this work, all engine-related turbomachinery is considered to be of the axial type.

The turbine cooling model of Gauntner [13] is adopted to estimate cooling air demand as a function of the maximum allowable turbine blade temperature and technology level.
The maximum allowable rotor blade temperature is estimated assuming creep as the dominant failure mechanism of the rotor blades and it therefore depends on material characteristics, blade stress and desired minimum lifetime for a certain amount of creep strain. For a given material, the relation between these variables can be modeled with the Larson-Miller Parameter LMP. The LMP is a function of blade temperature (T_{b}) at a given spanwise section of the blade and lifetime ($t_{\mathrm{b,life}}$) in hours for a given amount of creep strain: LMP = $T_{\mathrm{b}}[20 + log(t_{\mathrm{b,life}})]$. Creep strain is determined by the combination of blade stress and temperature. Both vary along the blade span. While the highest stress is experienced at the blade root, the highest blade temperatures are around mid-span. As a result the location of highest creep strain is located around a quarter or one third of the blade span [42, Ch. 9]. In this work creep stress is limited to 90% of creep rupture stress [42, Ch. 9] which corresponds to a creep strain of approximately 1% for single-crystal alloys according to Grieb [18, Ch. 5]. First-stage rotor blades experience the highest creep due to high centrifugal stress combined with very high temperatures. A simplified method is applied to determine rotor blade stress due to the centrifugal load at the root of the blade as outlined in [41]. Differently from the rotor blades, the implemented method assumes a constant value of maximum allowable temperature for the stator blades.

The dry mass of the engine excluding generators (m_{ts}) is estimated, to a first approximation, with an empirical correlation whose sole input is the corrected air mass flow rate at the compressor inlet ($\dot{m}_{0,\mathrm{red}}$). Data available in the database of Jane's [22] for 12 turboshaft engines in the 300-3000 kW power range are used to derive the following relation

$$m_{\mathrm{ts}} = 21.56 \cdot \dot{m}_{0,\mathrm{red}} + 85. \tag{6}$$

The mass resulting from this equation in combination with the considered engine power capacity results in mass-specific power values that are in good agreement with the technology assumptions cited by Schmollgruber et al. [43]. The mass of the generators is calculated by dividing the required take-off power with the mass-specific power value given in Tab. 3.

2.4.2 Design Assumptions

The thermodynamic design point of the engine is cruise (CR) at ISA+15 conditions. The overall pressure ratio (OPR) and turbine inlet temperature (TIT) that yield the highest efficiency at the design point are 45 and 1600 K, respectively. These values result from the requirement of keeping the high-pressure compressor (HPC) exit temperature during take-off below the allowable limit of 950 K [18]. The compression process is performed by a HPC with a pressure ratio of 20 and a low-pressure compressor (LPC) with a pressure ratio of 2.25.

The design point condition of the turbine cooling system is take-off (TO), when the highest value of TIT occurs. However, presently the framework is only capable of simulating a single design point of the CC-TS, which is cruise. To prevent an underestimation of the cooling air demand based on lower turbine temperatures during cruise, the temperature provided to the cooling model is multiplied by a correction factor. The value of this correction factor is approximated as $\theta_{0,\mathrm{to}}/\theta_{0,\mathrm{cr}} \approx \mathrm{TIT}_{\mathrm{to}}/\mathrm{TIT}_{\mathrm{cr}}$ [34], where θ_0 is the ratio of total free-stream temperature to static mean-sea-level temperature, assuming International Standard Atmosphere (ISA) conditions. The validity of this approach is verified by means of on/off-design simulations of the turboshaft engine. The cooling flow rate is also a function of the maximum allowable turbine blade temperature. A maximum allowable stator blade temperature of 1755 K is selected, assuming that the construction material is a ceramic matrix composite [24]. The single-crystal alloy TMS-238 is selected as the turbine blade metal and its characteristics are documented in Ref. [26]. Furthermore, a thermal barrier coating (TBC) is assumed to be applied to all blades and the temperature difference across the TBC is assumed to be 100 K [18].

The polytropic efficiencies are determined with the method of [18]. The values of average stage loading ($\bar{\Psi}$) are $\bar{\Psi}_{\mathrm{lpc}} = 0.8$, $\bar{\Psi}_{\mathrm{hpc}} = 1.0$, $\bar{\Psi}_{\mathrm{hpt}} = 3.5$, $\bar{\Psi}_{\mathrm{lpt}} = 3.5$, $\bar{\Psi}_{\mathrm{fpt}} = 3.5$. Note that $\bar{\Psi} = \frac{2\Delta H}{U_{\mathrm{m}}^2}$, where ΔH is the polytropic enthalpy change per stage and U_{m} the meridional velocity. Furthermore, 2035 is assumed as the entry into service (EIS) year of the investigated engine concept.

The cross-section of the exhaust duct of the engine is assumed to be of squared shape to accommodate the ORC evaporator. For each percent of pressure drop caused by the presence of the evaporator, the turboshaft thermal efficiency is reduced by approx. 0.2%. Therefore, a large evaporator frontal area is desirable as it reduces flow velocity and therefore pressure drop. However, the size of the evaporator needs to be limited to a reasonable level in order to be integrated into the nacelle of the engine. For this reason the side length of the exhaust duct is fixed to be approximately 20% larger than the power turbine exit diameter (see Fig. 7). The nozzle pressure ratio (Π_{noz}), which is defined as the ratio of the nozzle throat total pressure to ambient static pressure, is adopted as a design variable. Its value sets the amount of residual thrust ($F_{net,ts}$) that the engine generates. Producing thrust with the engines could be beneficial to counter the drag induced by the ram-air ducts housing the ORC condensers. Other design assumptions are made based on data provided by Mattingly et al. [34, Ch. 4] for an engine with EIS 2035, namely, that the air intake pressure loss is 0.2%, the combustor pressure loss is 4%, the high pressure and low pressure shaft mechanical efficiency is 99.6%, the FPT shaft mechanical efficiency is 98% and the nozzle pressure loss is 0.3%.

2.5 Organic Rankine Cycle Unit

The right side of Fig. 3 shows the PFD of the ORC system, based on an air-cooled non-recuperated configuration. To maximize thermodynamic efficiency a supercritical cycle is adopted. An in-house tool written in Python for on-design point thermodynamic cycle calculations is used for the analysis of the organic-Rankine-cycle. Thermodynamic properties of the working fluid, cyclopentane, are calculated with a state-of-the-art Helmholtz equation of state (HEOS) model implemented in the open-source library *CoolProp* [3], while the ideal gas model [7] is used for the turboshaft exhaust gas. Cyclopentane has a critical temperature (T_{crit}) of 512 K, a critical pressure (p_{crit}) of $45.1 \times 10^5 Pa$ and a normal boiling point temperature of 322 K [2]. According to results presented, for example, by Krempus et al. [28] cyclopentane is a suitable working fluid for an ORC system recuperating thermal energy from a gas turbine due to its high thermal stability ($T_{max,fluid}$) of 573 K and high T_{crit}. It is however possible that cyclopentane is not the optimal working fluid, both in terms of performance of the resulting system and other technical and safety considerations. Alternative working fluids will be assessed in future works.

The ORC turbine gross power output ($\dot{W}_{gross,orc}$) is converted into electrical power via a dedicated generator (see Figure 4). The turbine mechanical efficiency ($\eta_{mech,turb}$) and ORC generator efficiency ($\eta_{gen,ORC}$) are an output of the turbogenerator design procedure described in Section 2.6. For the pump, an isentropic pump efficiency ($\eta_{is,pump}$) of 65% and a mass-specific power of 4 kW/kg are assumed. These values are taken from Kwak et al. [30] which documents research on electrically driven centrifugal pumps for small space launch vehicles, which operate under similar conditions as expected for the pump of the ORC unit. The efficiency of the pump motor ($\eta_{mot,pump}$) is taken from Tab. 3. Furthermore, a pump mechanical efficiency ($\eta_{mech,pump}$) of 99% is assumed. The net power output of the ORC waste-heat-recovery system ($\dot{W}_{net,orc}$) is defined as

$$\dot{W}_{net,orc} = \dot{W}_{gross,orc}\eta_{mech,turb}\eta_{gen,orc} - \frac{\dot{W}_{net,pump}}{\eta_{mech,pump}\eta_{mot,pump}}. \tag{7}$$

The ORC system mass (m_{orc}) is determined as the sum of pump mass (m_{pump}), turbogenerator mass (m_{tg}), condenser mass (m_{cond}), evaporator mass (m_{evap}), working fluid mass (m_{fluid}) and balance-of-plant mass ($m_{bop,orc}$). The heat exchanger and turbogenerator masses are an output of the corresponding modules performing their preliminary design. m_{fluid} is estimated as the product of 1.2 times the evaporator cold side volume and the density of the working fluid at one atmosphere and 25 °C. It is further assumed that $m_{bop,orc}$ constitutes 10% of m_{orc}. This value is similar to that taken by Zarati et al. [50]. However, the value assumed for the mass of the balance-of-plant components is affected by uncertainty given the lack of information regarding ORC systems design for airborne applications.

The ORC unit is designed for the same environmental conditions as the turboshaft engine, i.e., CR ISA+15. Table 4 lists the ORC thermodynamic cycle specifications and indicates the input values which are output values of other sub-models.

2.6 ORC Turbogenerator

The ORC turbogenerator is modelled by means of an in-house Python program for the preliminary design of high-speed turbomachinery. The code has been used for the preliminary design of a 10 kW laboratory high-speed ORC turbine being realized at Delft University of Technology. The turbogenerator consists of the radial-inflow turbine, the circular cross-section volute guiding the flow at the turbine inlet, and a permanent-magnet generator.

The model employed to design the single-stage radial-inflow turbine is based on an iterative routine based on the theoretical framework described by Chen and Baines [6]. All flow losses (internal and external) occurring in the stage are modelled by means of low-order physical models, equivalent to those adopted by Giuffré and Pini [15] for

Table 4: ORC thermodynamic cycle specifications

Parameter	Input	Parameter	Input	Parameter	Input
$T_{\mathrm{max,orc}}$	Design variable	$\Delta p_{\mathrm{h,ecap}}$	HEX model	$\eta_{\mathrm{is,pump}}$	65%
$T_{\mathrm{min,orc}}$	Design variable	$\Delta p_{\mathrm{c,evap}}$	HEX model	$\eta_{\mathrm{is,turb}}$	Turbogenerator model
$p_{\mathrm{max,orc}}$	Design variable	$\Delta T_{\mathrm{pp,evap}}$	Design variable		
$T_{\mathrm{c,cond,in}}$	Ram-duct model	$\Delta p_{\mathrm{h,cond}}$	HEX model		
$\dot{m}_{\mathrm{h,evap}}$	Turboshaft model	$\Delta p_{\mathrm{c,cond}}$	HEX model		
$T_{\mathrm{h,evap,in}}$	Turboshaft model	$\Delta T_{\mathrm{pp,cond}}$	Design variable		

Note: Subscripts h and c indicate heat exchanger (HEX) hot and cold sides.

axial turbine stages. Volute losses are computed using the model proposed by Japikse [23] for centrifugal compressors and adapted to the case of turbine volutes. Fluid thermodynamic properties are calculated with a commercial software library [33]. The combined impeller and volute mass is determined based on an automatically generated and simplified computational aided design model generated by the program. In this procedure, rotor and stator blade masses are neglected and the volute is treated as a hollow toroidal duct. The wall thickness of the components volute, stator base plate and impeller shroud is set to 5 mm. This value is based on engineering practice and manufacturing considerations.

The generator is assumed to be a cylindrical FeCo-based permanent-magnet machine with a carbon fiber retaining sleeve. The electromagnetic power of the generator and its windage loss within the air gap are modelled according to the method of James and Zahawi [21] using optimized machine-specific parameters documented by van der Geest et al. [48]. The mass-specific power is computed by interpolation using data from Ref. [48] expressed as a function of the rotor surface velocity. The total mass of the generator system is obtained by summing the mass of the generator, the mass of its power electronics and the mass of the DC-DC converter. The individual component masses are calculated by dividing the electromagnetic power by the mass-specific power. Values of state-of-the-art mass-specific power related to the power electronics and to the DC-DC converter are taken as 14.3 kW/kg and 62.0 kW/kg, respectively. These values are obtained from the work of Gesell et al. [14]. The turbogenerator mass (m_{tg}) is the sum of generator system mass, radial-inflow turbine mass and volute mass.

The turbogenerator preliminary design tool requires as input the total inlet pressure and temperature, the total-to-total stage pressure ratio and the design mass flow rate. The main output variables are the turbine total-to-total efficiency ($\eta_{\mathrm{is,turb}}$), the turbine mechanical efficiency ($\eta_{\mathrm{mech,turb}}$), the generator efficiency ($\eta_{\mathrm{gen,orc}}$), and the m_{tg}.

2.7 Heat Exchangers

Figure 5 shows the chosen topology for the ORC evaporator, namely a multi-pass inline bare-tube bundle heat exchanger where the working fluid flows inside the tubes in a counter-crossflow arrangement with respect to the exhaust gases. The nickle-base alloy Hastelloy X® is selected as construction material owing to its good oxidation resistance, manufacturability, and strength at the high temperatures [18]. The tube outer diameter is set to 1.8 mm, while the tube thickness is calculated given the pressure difference between the working fluid and the exhaust gases. The evaporator optimization variables are the non-dimensional transversal pitch ($x_{\mathrm{t,evap}}$), the non-dimensional longitudinal pitch ($x_{\mathrm{l,evap}}$) and the number of passes ($n_{\mathrm{pass,evap}}$).

The condenser is a flat-tube-microchannel heat exchanger with louvered fins (see Fig. 6). Based on manufacturability considerations the following values are fixed: fin thickness 0.11 mm, flat tube thickness 0.2 mm, height of the microchannels 1.6 mm. Furthermore, the louver fin length and louver pitch are set to be 90% of the fin height and fin pitch, respectively. The condenser optimization variables are the fin height ($b_{\mathrm{f,cond}}$), the fin pitch ($p_{\mathrm{f,cond}}$), the louver angle ($\phi_{\mathrm{l,cond}}$) and the length of the flat-tubes (X_{cond}). Based on the estimated space demand for the turboshaft engine inside the nacelle the condenser width (Y_{cond}) is fixed to 1.5 m (see Fig. 7). An aluminium alloy of the 3000 series is selected as the construction material, as suggested in the technical report of Kaltra GmbH [25].

The in-house Python tool *HeXacode* is used for heat exchanger sizing. The program was verified by comparison with a commercial code for heat exchanger design and rating [17]. The sizing procedure consists in calculating the required heat transfer area for a given heat duty, given the inlet temperature, pressure, and mass flow rate of the hot and cold streams. The outputs are the heat exchanger dimensions, mass, and pressure drops of the cold and hot sides. For both the evaporator and the condenser, the frontal area is an input, while the depth is calculated to meet the design specifications. In case of the condenser, this corresponds to determining the number of microchannels within a single flat tube and in case of the evaporator the number of streamwise tubes per pass. For both heat exchanger types, the geometry is discretized into several control volumes in which mean values of the fluid thermodynamic properties and the corresponding heat transfer and friction coefficients are evaluated. The evaporator features a multi-pass layout and

the number of cells is set equal to the number of passes. The condenser is discretized into three volumes representing the different phases the working fluid undergoes (superheated vapour, two-phase fluid, sub-cooled liquid). The heat transfer correlations are formulated in terms of Colburn factor or Nusselt number and the pressure drop calculation is based on the estimate of the friction factor or the pressure gradient. The design calculation stops when the relative difference in the calculated overall heat transfer area between two consecutive iterations is smaller than 1%.

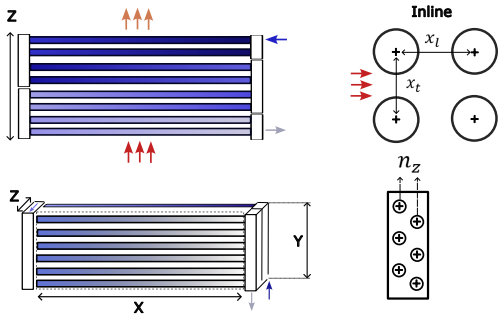

Figure 5: Evaporator core geometry: multi-pass inline bare tube bundle.

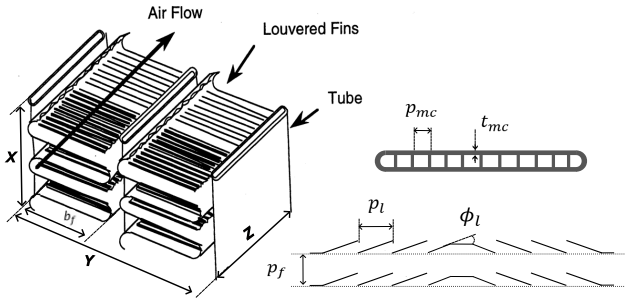

Figure 6: Condenser core geometry: Flat tube microchannels with louvered fins.

2.8 Ram-air Duct

The ram-air duct houses the condenser of the ORC unit and provides it with ambient air for cooling. It consists of an intake, a diffuser, a duct accommodating the heat exchanger and a convergent nozzle. Figure 7 gives an overview of the main components of the ram-air duct and how they are arranged in the CC-TS configuration. The ram-air duct model allows to compute internal losses and external losses due to friction and pressure drag, as well as thermal energy input to the air flow due to the condensing fluid in the heat exchanger. The model is based on the compressible duct model of the Python library *openConcept* [1] and is coupled with loss models for the intake, the diffuser, and pressure losses arising from heat exchanger tilt. The thermal energy input results from the simulation of the ORC system on-design operation and the condenser cold side pressure loss is computed according to the procedure described in Section 2.7. The expansion through the nozzle of the duct is considered isentropic.

A subsonic scoop intake is assumed and its pressure recovery and drag are estimated using the method reported in Ref. [12]. This method considers drag contributions due to skin friction, spillage drag and diverter drag. With reference to Fig. 7, due to the location of the ram-air duct on the nacelle, the boundary layer thickness along the short part of the nacelle in front of the intake is neglected, as well as the possible presence of a diverter. The drag of the intake as well as the pressure recovery is a function of the intake design mass flow fraction ($\dot{m}_{\text{frac,intake}}$), which is defined as the geometrical intake area A_1 divided by the stream tube area (A_0) ahead of the intake (see Fig. 7). A value of $\dot{m}_{\text{fraction}} < 1$ results in an isentropic compression of the incoming airflow ahead of the intake. This reduces the Mach number at the entry to the intake and therefore increases the internal pressure recovery. However, spillage drag occurs. A value of $\dot{m}_{\text{fraction}} = 1$ results in zero spillage drag but no isentropic compression ahead of the intake and an increased intake Mach number which results in lower internal pressure recovery. Therefore, the selection of $\dot{m}_{\text{frac,intake}}$ depends on a trade-off between internal and external losses and, for this reason, its optimal value is selected by the optimizer (see Tab. 2).

The intake is followed by a rectangular diffuser. The total pressure losses are calculated based on the ratio of the actual pressure over the ideal pressure recovery coefficient and depend on the diffuser area ratio $AR_{\text{diff}} = A_2/A_1$ [44]. While the diffuser entrance area (A_1) is calculated from the intake specifications and the required mass flow rate, the diffuser exit area (A_2) depends on both the heat exchanger frontal area (A_3) and its tilt angle (θ_{cond}). θ_{cond} is defined as the angle between the normal of the heat exchanger frontal area plane and the core duct velocity direction (see Fig. 7). A higher value of θ_{cond} is beneficial with respect to the frontal area of the heat exchanger, if duct cross sectional area is limited. This also reduces the required AR_{diff} and therefore results in less diffuser pressure loss. However, a larger tilt angle requires more deflection of the air stream, therefore it implies additional drag. The additional pressure loss arising due to the heat exchanger tilt is modeled based on a fit of experimental results reported by Nichols [35]. The heat exchanger inlet conditions are calculated assuming an isentropic expansion from the diffuser exit (A_2 in Fig. 7) to the heat exchanger inlet (A_3 in Fig. 7).

2.9 CC-TS Integration

The addition of an ORC WHR system to a turboshaft engine not only involves a mass addition but also demands for additional space, which is limited onboard an aircraft. Volume limitations mainly affect the integration of the ORC heat exchangers, posing a strong limitation on their performance, as the optimal heat transfer surface is bound to be smaller than the optimal value if unconstrained by the volume limitation. Therefore, the integration of the ORC unit within the aircraft is of key importance. Figure 7 depicts a preliminary concept regarding the integration of the ORC heat exchangers into the nacelle containing the turboshaft engine and generators. A single evaporator is located right after the free power turbine in a square-shaped duct extending to approximately 1.2 times the diameter of the engine. Two condensers are integrated into the nacelle of the turboshaft engine. Tilting the condensers allows to keep the frontal area of the assembly as small as possible. The maximal width of the condenser (Y_{cond}) is given by the engine and generator size requirements. Note that no information is available on how the generators are integrated into the nacelle of the ONERA Dragon.

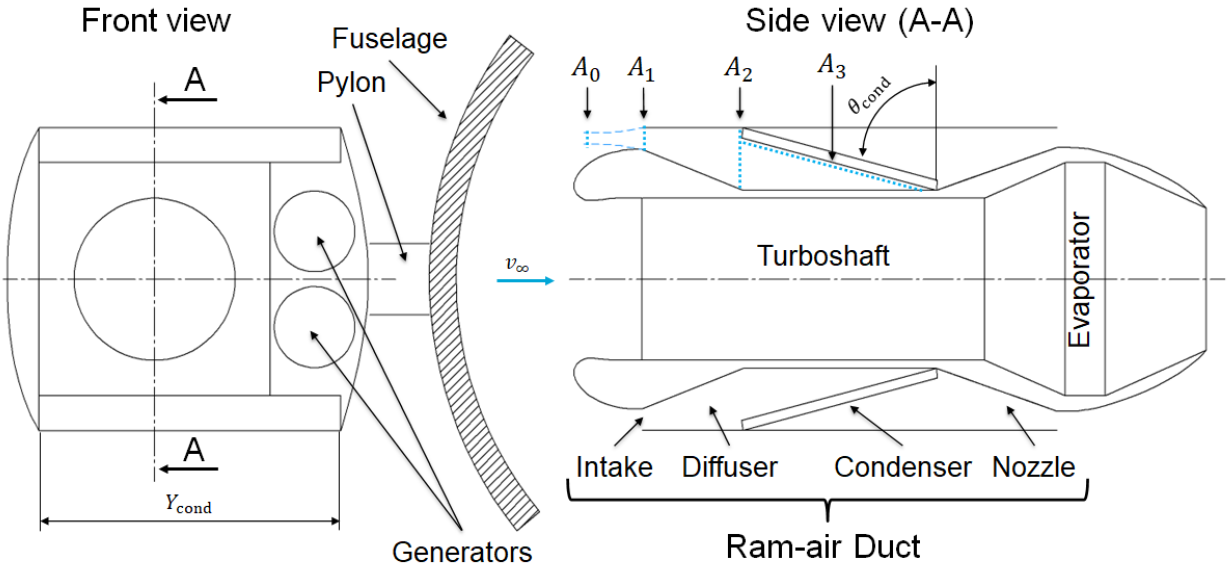

Figure 7: Preliminary concept of the integration of the ORC WHR unit and the turboshaft engine within the nacelle in the aft of the aircraft. Variables A_0, A_1, A_2 and A_3 indicate the cross sectional areas along ram-air duct flow path.

3. RESULTS AND DISCUSSION

The ARENA framework is first verified by simulating the ONERA Dragon aircraft and comparing the results with published data related to this aircraft concept [43]. Secondly, the verified framework is used to compute the performance of a Dragon-type aircraft equipped with the optimized CC-TS engines and the result is compared with a reference aircraft. The top level aircraft requirements (TLARs) of all considered aircraft are the same as those of the ONERA Dragon and are listed in Tab. 1.

3.1 Verification Case

Two verification cases are simulated. They differ in the value of power specific fuel consumption during cruise ($\text{PSFC}_{\text{net,cr}}$), while the TLARs remain the same as listed in Tab. 1. For verification case nr. 1 $\text{PSFC}_{\text{net,cr}}$ is fixed to a value of 0.145 kg/(kWh) and m_{pt} to 9.40 t, which are values derived from data regarding the ONERA Dragon provided by Schmollgruber et al. [43]. Schmollgruber et al. [43] assume a 10% improvement in PSFC over an engine designed in the year 2020. However, no details on the technological advancements necessary to achieve this reduction in PSFC are given. Therefore, a different value of PSFC has to be expected when using he engine model described in Section 2.4. For verification case nr. 2 $\text{PSFC}_{\text{net,cr}}$ is calculated using the engine model and the modelling assumptions stated in Section 2.4. The value of Π_{noz} is set to 1.17, to obtain an almost zero net thrust production by the turboshaft engine. Table 5 compares the results of the verification cases with the data of the ONERA Dragon provided

by Schmollgruber et al. [43].

The comparison shows that verification case nr. 1 is in good agreement with the data reported for the ONERA Dragon. This verifies that the ARENA framework is able to compute the main characteristics of the aircraft with a sufficient degree of accuracy. Based on the modelling assumptions of verification case nr. 2, the turboshaft engine has a $PSFC_{net,cr}$ that is approximately 10% larger than the value reported for the ONERA Dragon. This leads to an increase in fuel consumption of 13% and an overall heavier and larger aircraft. The reference aircraft simulated and compared with the optimized Dragon CC-TS concept in Section 3.2 differs in a similar way from the ONERA Dragon.

Table 5: Comparison of the results obtained with the developed simulation framework with the data published for the ONERA Dragon [43]

Parameter	**ONERA Dragon**	**Verification Case 1**	**Delta**	**Verification Case 2**	**Delta**
m_{mto} (t)	67.9	68.2	0.4%	69.5	2.4%
m_{oe} (t)	42.7	42.8	0.2%	42.8	0.2%
m_{pt} (t)	9.40*	9.40	0.0%	9.29	-1.2%
m_{wing} (t)	8.40*	8.51	1.3%	8.64	2.9%
m_{fuel} (t)	11.5	11.8	2.6%	13.1	13.9%
L/D (-)	17.2	17.2	0.0%	17.2	0.0%
S_{ref} (m^2)	121	122	0.8%	124	2.5%
b (m)	36.0	36.1	0.3%	36.5	1.4%
$PSFC_{net,cr}$ (kg/kWh)	0.145	0.145	0.0%	0.159	9.7%
$\dot{W}_{cr}$ (MW)	10.5**	10.8	-2.9%	10.9	3.8%
$\dot{W}_{to}$ (MW)	23.2	23.3	0.4%	23.7	2.2%

* Approximated based on data given in Ref. [43]

** Approximated based on data given in Ref. [43] and propulsive efficiency given by Defoort et al. [11]

3.2 Optimized Dragon CC-TS

The optimized Dragon CC-TS and the reference aircraft adopt the same powertrain architecture (Fig. 4 and only differ in the used engine type. Both the CC-TS and the simple-cycle turboshaft engines of the reference aircraft are based on the design assumptions given in Section 2.4. Table 6 shows a comparison between the main performance parameters of the optimized Dragon CC-TS aircraft and those of the reference aircraft. Furthermore, Tab. 7 displays the optimized design vector calculated for the Dragon CC-TS. In the case of the reference aircraft, Π_{noz} is selected as the only design variable and its optimum value for minimum fuel consumption is determined to be 1.35.

The simulation of the aircraft powered by the optimized CC-TS results in an improvement of the estimated PSFC (Eq. 5) of 6.5% and a reduction of mission fuel consumption (m_{fuel}) of 1.5% if compared to the reference aircraft. m_{fuel} is a function of $\dot{m}_{fuel}$ which is computed as the product of PSFC and $\dot{W}_{cr}$. While the PSFC of the Dragon CC-TS is 6.5% lower than that calculated for the reference aircraft, its $\dot{W}_{cr}$ is 4.9% higher (see Section 3.2.1). As a result the percentage of fuel saving is smaller than the improvement of PSFC. The powertrain mass of the Dragon CC-TS is 460 kg heavier than that of the reference aircraft, which is mainly due to the added mass of the ORC unit. Despite the resulting increase in m_{oe} wing mass (m_{wing}) does not vary appreciably. Furthermore, the increase in empty mass of the Dragon CC-TS is balanced by a fuel mass reduction of 200 kg which results in the values of m_{mto} being similar for both aircraft. The lift-to-drag ratio (L/D) of the Dragon CC-TS is slightly higher due to thrust production by the ram-air ducts which is considered as a reduction in zero-lift drag (see Section 2.2). The reference aircraft and the Dragon CC-TS aircraft are both larger aircraft in terms of mass and wing size compared to the ONERA Dragon. This is due to the engine design assumptions as explained in Section 3.1. The larger wing area combined with a fixed wing aspect ratio (see Section 2.2) result in a slight violation of the wing span limit of 36 m that is taken as a constraint for the ONERA Dragon design. This limit is not a certification requirement for the aircraft, but a limit imposed by airport gate size for Airbus A320-sized aircraft. However, in order not to restrict the design space unnecessarily, it is not imposed as an optimization constraint.

Figure 8 reports the mass breakdown of the CC-TS engine and Fig. 9 the simplified temperature-entropy diagram of the ORC. The overall mass of the optimized CC-TS is 1710 kg , of which 1450 kg or 85% account for the mass of the turboshaft engine and of the two engine-mounted generators, while the estimated mass of the ORC unit is 260 kg or

15% of the total mass. $\dot{W}_{cr}$ of a single CC-TS engine is 5.42 MW, of which 5.08 MW is the electric power output of the engine mounted generators and 335 kW is the net electric power output of the ORC unit. The resulting mass-specific power of the CC-TS, turboshaft engine including generators and ORC unit are 3.2 kW/kg, 3.5 kW/kg and 1.3 kW/kg, respectively. The thermal efficiencies of the CC-TS, turboshaft and ORC unit are $\eta_{net,ccts} = 53.2\%$, $\eta_{net,ts} = 49.9\%$ and $\eta_{net,orc} = 17.2\%$, respectively. The working fluid mass flow rate of the ORC system is 3.3 kg/s and the cooling air requirement is 8.9 kg/s per condenser. One single CC-TS unit is equipped with two condensers (see Fig. 7). The condenser has a dimension of $1.0 \times 1.5m \times 0.07$m (see Fig. 7 where the schematic representation of the heat exchanger is approximately at scale) and a mass of 38 kg. The condenser cold-side pressure drop ($\Delta p_{c,cond}$) is 730 Pa and it rejects a thermal power of 800 kW to the atmosphere, which causes the the cooling air to undergo a temperature rise of 90 K. As a result the ram-air duct generates a net thrust of 20 N which stems from a thrust attributed to internal forces of 200 N and a drag attributed to external forces of 180 N. The mass of the evaporator is 48 kg and it has dimensions of $1.1 \times 1.1 \times 0.1$m (see Fig. 7 where the schematic representation of the heat exchanger is at approximate scale). The evaporator recovers a thermal power of 1.94 MW. The mass flow rate of the gas turbine exhaust is 11.2 kg/s, the hot exhaust gases enter the evaporator at a temperature $T_{h,evap,in} = 670$ K and leaves it at 500 K. The evaporator hot side pressure drop ($\Delta p_{h,evap}$) is 2060 Pa which amounts to 6% of the FPT exit total pressure. The optimized ORC radial-inflow turbine design has an efficiency ($\eta_{is,turb}$) of 95%, a speed of 74 500 rpm and a gross power output ($\dot{W}_{gross,orc}$) of 390 kW. The ORC turbogenerator mechanical efficiency ($\eta_{mech,turb}$) is 99% and the generator efficiency ($\eta_{gen,orc}$) is 97%. The ORC turbogenerator mass (m_{tg}) is 83 kg, thus it accounts for about one third of the overall ORC system mass. After accounting for turbine mechanical losses and generator efficiency the net power output of the turbogenerator is 370 kW and its mass specific power is 4.5 kW/kg. The net power requirement of ORC pump ($\dot{W}_{net,pump}$) is 38 kW.

Table 6: Comparison of the optimized Dragon CC-TS with the reference aircraft

Parameter	**Reference Aircraft**	**Dragon CC-TS**	**Delta**
m_{mto} (t)	69.4	69.7	0.4%
m_{oe} (t)	42.8	43.3	1.2%
m_{pt} (t)	9.26	9.72	5.0%
m_{wing} (t)	8.62	8.69	0.8%
m_{fuel} (t)	13.0	12.8	-1.5%
L/D (-)	17.2	17.3	0.6%
S_{ref} (m^2)	124	125	0.8%
b (m)	36.4	36.5	0.3%
$PSFC_{net,cr}$ (kg/kWh)	0.168	0.157	-6.5%
$\dot{W}_{cr}$ (MW)	10.3	10.8	4.9%
$\dot{W}_{to}$ (MW)	23.7	23.8	0.4%

Table 7: Design vector of the optimized Dragon CC-TS

Parameter	Π_{noz}	$T_{min,orc}$	$T_{max,orc}$	$p_{max,orc}$	$\Delta T_{pp,cond}$	$\Delta T_{pp,evap}$	X_{cond}	$\phi_{l,cond}$	$b_{f,cond}$
Value	1.27	398 K	549 K	54.4 bar	41.8 K	97.8 K	1.00 m	29.7°	10.1 mm
Parameter	$p_{f,cond}$	$x_{t,evap}$	$x_{l,evap}$	$n_{pass,evap}$	$\dot{m}_{frac,intake}$	θ_{cond}	Ψ_{is}	Φ	ν
Value	1.41 mm	3.00	1.25	9	0.670	59.4°	0.966	0.394	0.460

3.2.1 Results Discussion

Table 7 lists the optimized design vector of the Dragon CC-TS aircraft. The values of the design variables result from the complex mutual interaction of all sub-modules. For example, from a thermodynamic standpoint, ORC efficiency is maximized by maximizing $T_{max,orc}$ and $p_{max,orc}$ and minimizing $T_{min,orc}$. However, the requirements associated with the integration of the ORC unit within the nacelle result in values for these design variables that differ from their thermodynamically optimal values, and lie between the respective lower and upper bounds specified in Tab. 2.

The pressure loss in the exhaust duct of the turboshaft caused by the evaporator ($\Delta p_{h,evap}$) is 6% and it reduces the turboshaft thermal efficiency by approximately 1.2%. As mentioned in Section 2.4.2, the evaporator frontal area

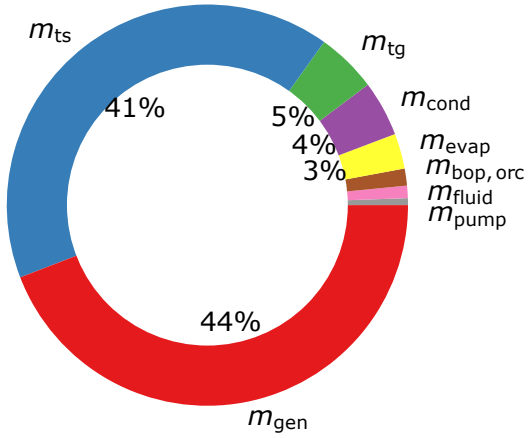

Figure 8: CC-TS mass breakdown; The engine generator mass m_{gen} and the condenser mass m_{cond} account for two units each.

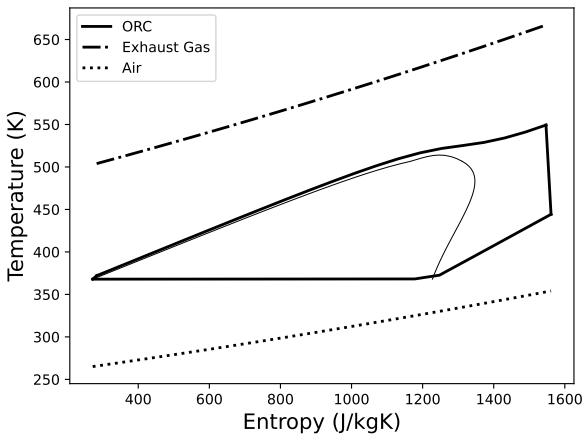

Figure 9: Temperature-entropy diagram of the ORC including engine exhaust gas and cooling air.

is larger than the FPT outlet area. This results in a lower bulk flow velocity and therefore pressure loss. Furthermore, the evaporator optimization variables adopt values to minimize $\Delta p_{h,evap}$. The lowest pressure drop is achieved with the maximum value of $x_{t,evap}$ and the minimum value of $x_{l,evap}$. This configuration minimizes detached flow behind each tube and therefore pressure loss. The number of passes ($n_{pass,evap}$) is the minimum value because this variable has little effect on the evaporator number of tubes, and thus on $\Delta p_{h,evap}$. A higher number of passes would only lead to a higher working fluid pressure drop. Finally, the evaporator pinch point difference ($\Delta T_{pp,evap}$) is maximum because it reduces the required evaporator heat transfer area and therefore $\Delta p_{h,evap}$.

Despite the optimized evaporator design, the resulting configuration entails several disadvantages. First, a diffuser is necessary to connect the FPT outlet to the evaporator. This not only adds length and mass to the system but also causes additional pressure loss due to diffusion. Secondly, the increase in evaporator area and therefore the potential to reduce pressure loss is limited by the additional nacelle drag as a result of an increase of propulsion system size.

While the evaporator only influences the thermodynamic performance of the CC-TS, the condenser additionally interacts with the aircraft aerodynamics via the net force produced by the ram-air duct. The present results show that it is possible to balance internal and external ram-air duct drag with the production of thrust due to heat addition to the air flow, provided that the duct is properly designed. To achieve this benefit, optimal design variable values for the condenser are those that provide a balance between the heat transfer area, the heat transfer coefficient and the air-side pressure drop ($\Delta p_{c,cond}$). The optimizer therefore selects the condenser design with the maximum frontal area to reduce the flow velocity and therefore $\Delta p_{c,cond}$. The optimization process highlights that it is more beneficial to add heat transfer area by increasing the flat-tube length (X_{cond}) and by tuning the fin parameters instead of increasing the depth, which linearly increases the pressure drop. Similarly, a maximization of the free-flow-to-frontal-area ratio of the condenser reduces the channel flow acceleration and, therefore, the maximum velocities and the pressure drop. This result is achieved by reducing the number of flat-tubes which entails that the condenser fin height $b_{f,cond}$ is maximized. Conversely, the fin pitch $p_{f,cond}$ is minimized in order to keep the heat transfer area to suitable values, and this causes a minimal pressure drop penalty. Additionally, the ram-air duct adopts a large diffuser area ratio (AR_{diff}) to reduce the condenser face velocity as much as possible. AR_{diff} adopts a value that is close to 6 which is the upper limit of the used correlation.

As a consequence of the heat exchangers impact on turboshaft efficiency and aircraft drag, the performance of the ORC unit is limited. This results in a $\dot{W}_{net,orc}$ that only accounts for approximately 5% of cruise power demand. To summarize the discussion above, the need to keep heat exchanger gas-side pressure drops as low as possible results in: 1) high pinch point temperature differences which reduce the amount of heat exchanged with the exhaust gas and the ram-air and 2) an increase in $T_{min,orc}$ which reduces ORC efficiency. This highlights the impact of heat exchanger selection and integration on system performance and the mutual dependency between different parts of the system.

The working fluid is an important degree of freedom in the design of ORC systems [8], the thermodynamic cycle parameters, the conversion efficiency, the design of the components, and their techno-economic performance (turbine, heat exchangers, pump), depend on it. As briefly mentioned in Section 2.5, cyclopentane is selected as the

working fluid because previous research [28] indicated that it satisfies many of the requirements for stationary WHR applications in this power range. For this reason it was already selected as the working fluid in a previous study on a combined-cycle auxiliary power unit [29]. However, the exhaust gas temperature of the turboshaft engine considered in this work (670 K) is lower than the exhaust gas temperature of the stationary gas turbine (760 K) studied by Krempus et al. [28]. The difference in temperature is due to the higher thermal efficiency of the turboshaft engine. Further investigation is therefore required in the optimal selection of the ORC working fluid for highly efficient aircraft gas turbine engines.

The generator output power required during cruise ($\dot{W}_{\mathrm{cr}}$) by the reference aircraft is 4.9% lower than that required by the Dragon CC-TS, despite similar mass and L/D. This difference is caused by the different amount of residual thrust ($F_{\mathrm{net,ts}}$) produced by the turboshaft engines of the reference aircraft with respect to the CC-TS engines. $F_{\mathrm{net,ts}}$ affects the required $\dot{W}_{\mathrm{cr}}$ according to Eq. 3. The $F_{\mathrm{net,ts}}$ of a single engine amounts to 970 N for the reference aircraft and 170 N for the Dragon CC-TS. The engine residual thrust is set by the nozzle pressure ratio (Π_{noz}) which is an optimization parameter in both cases. The optimum value of Π_{noz} depends on the exhaust duct pressure losses ($\Delta p_{\mathrm{h,evap}}$), on the exhaust duct heat extraction ($\dot{Q}_{\mathrm{evap}}$), as well as on propulsive efficiency (η_{prop}). For the studied engine configuration a value of Π_{noz} in the range of approximately 1.0-1.2 results in a negative $F_{\mathrm{net,ts}}$ and therefore an increased demand of $\dot{W}_{\mathrm{cr}}$. A parametric study of the turboshaft model considering variations of the parameters $\Delta p_{\mathrm{h,evap}}$, $\dot{Q}_{\mathrm{evap}}$ and η_{prop} shows that optimal values of Π_{noz} always lead to a positive value of $F_{\mathrm{net,ts}}$. Furthermore, with increasing η_{prop}, the optimal value of Π_{noz} reduces as the thrust is more efficiently generated by the powertrain if electric power is deliverer to the ducted-fans than if it is generated by the exhaust jet. These results highlight that it is important to consider the impact of Π_{noz} on the overall system performance.

3.2.2 Methodology Limitations

Possible improvements and limitations of the methodology are as follows.

- The current powertrain model does not consider the cooling requirements of electrical components. Especially the turboshaft-mounted generators, with a rated power of approximately 6 MW, require active cooling during take-off. The variation in mass and power requirement of this system is not included in the current analysis. As explained in Section 2.3 the cooling system mass is assumed constant and included in the aircraft mass m'_{oe}.
- The aircraft model does not consider the variation of the nacelle size and drag with respect to engine size. It can be argued that the baseline drag polar of the reference aircraft includes the contribution of the nacelle. However, in case of the CC-TS, modifications to the nacelle are necessary. The current modelling approach only considers a change in wetted area of the nacelle by the ram-air duct model. Furthermore, nacelle and ram-air duct mass are neglected.
- Fluid dynamic losses related to the engine exhaust duct are only partially modelled. For example, losses encountered in the diffuser connecting the FPT outlet to the evaporator are not accounted for. Furthermore, a physics-based modelling of the engine's nozzle losses is missing.
- The CC-TS system schematic of Fig. 7 shows that according to this conceptual arrangement the generators are connected to the FPT via a radial drive shaft similar to the ones adopted for secondary power off-takes of turbofan engines. However, the use of a high-speed generator might allow for the direct coupling of the generator with the FPT shaft. Such a direct coupling may affect the air intake or nozzle flow path if the generators are placed on the centerline of the engine. Therefore, the integration of the generators with the turboshaft engines and its impact on propulsion system size and performance requires further investigation.
- The objective of the present work is to identify a propulsion system that is environmentally friendlier than conventional gas turbine engines. Mission fuel consumption is selected as the figure of merit to assess the environmental impact. However, while uncertainty is still large, most recent research suggests that non-CO_2 emissions, such as the emission of NOx and water vapor, account for two thirds of radiative forcing caused by aviation [32]. Therefore, to identify a CC-TS design that results in the least climate impact, it is necessary to extend the current framework to also account for non-CO_2 emissions. In this case a suitable figure of merit can be the average temperature response suggested by Dallara et al. [9].

4. CONCLUSIONS

The work documented here is an initial feasibility investigation about the concept of a novel power unit for turbolectric aircaft based on the concept of a combined cycle engine formed by a turboshaft engine and an organic-Rankine-cycle (ORC) waste-heat-recovery (WHR) system. This novel aircraft architecture is investigated by means of a newly developed multidisciplinary simulation framework encompassing the modeling of the complex powertrain and of the

main design elements of the aircraft in order to estimate the merit parameters of the new aircraft over a representative mission. In particular, this framework allows to compute the thermodynamic performance of the combined cycle engine, performs the preliminary design of the components, and considers changes to the aircraft aerodynamics and operating empty mass due to the addition of the new system. An optimal design of the combined cycle turboshaft engine (CC-TS) is identified using a genetic algorithm. The optimization objective is the minimization of the mission fuel mass based on the variation of 18 design variables. The investigated aircraft configuration is similar to that of the ONERA Dragon concept. It is shown that a reduction of mission fuel mass of 1.5% is possible if the turboelectric powertrain is equipped with a CC-TS instead of a simple-cycle turboshaft engine. The increase in operating empty mass of the aircraft employing the CC-TS due to its heavier powertrain is balanced by the reduction in fuel mass, which results in both the reference aircraft and the new concept having a similar take-off mass. Furthermore, calculations demonstrate that the drag resulting from the ram-air duct which houses the condenser of the ORC unit can be balanced by thrust generated due to thermal energy addition to the air stream. Heat exchanger size limitations and the need to keep gas-side pressure drop as low as possible is identified as the most critical performance limitation of the ORC WHR unit. Based on these findings, future work will investigate:

- different condenser topologies to reduce air-side pressure drop,
- different evaporator layouts that allow reduced gas-side pressure drop while keeping engine frontal area as small as possible,
- different ORC architectures, e.g., adopting a recuperator could allow a reduction in condenser size and subsequently a potential reduction in drag due to ram-air ducts in case of an air-cooled ORC configuration,
- different ways to utilize the power provided by the ORC turbine, e.g., via mechanical coupling with the turboshaft engine,
- the identification of an optimal ORC working fluid for airborne WHR applications,
- the optimal integration of the ORC system with the gas turbine engine and airframe, and
- the identification of an optimized CC-TS design for minimized environmental impact including non-CO_2 effects.

ACKNOWLEDGEMENT

This research has been supported by the Applied and Engineering Sciences Division (TTW) of the Dutch Organization for Scientific Research (NWO), Open Technology Program of the Ministry of Economic Affairs, Grant No. 17906.

References

[1] E. J. Adler and J. R. R. A. Martins. Efficient Aerostructural Wing Optimization Considering Mission Analysis. *Journal of Aircraft*, 2022. doi: 10.2514/1.c037096.

[2] M. Astolfi and E. Macchi. *Organic Rankine Cycle (ORC) Power Systems*. Elsevier, 2017. doi: 10.1016/c2014-0-04239-6.

[3] I. H. Bell, J. Wronski, S. Quoilin, and V. Lemort. Pure and Pseudo-pure Fluid Thermophysical Property Evaluation and the Open-Source Thermophysical Property Library CoolProp. *Industrial & Engineering Chemistry Research*, 53(6):2498–2508, 2014. doi: 10.1021/ie4033999.

[4] J. Blank and K. Deb. Pymoo: Multi-Objective Optimization in Python. *IEEE Access*, 8:89497–89509, 2020. ISSN 21693536. doi: 10.1109/ACCESS.2020.2990567.

[5] S. Boggia and K. Rüd. Intercooled Recuperated Gas Turbine Engine Concept. Tuscon, Arizona, USA, 7 2005. 41st AIAA/ASME/SAE/ASEE Joint Propulsion Conference Exhibit. doi: 10.2514/6.2005-4192.

[6] H. Chen and N. C. Baines. The Aerodynamic Loading of Radial and Mixed-flow Turbines. *International Journal of Mechanical Sciences*, 36:63–79, 1 1994. doi: 10.1016/0020-7403(94)90007-8.

[7] P. Colonna and T. van der Stelt. FluidProp (Version 3.1): A program for the estimation of thermophysical properties of fluids, 2019. URL `https://asimptote.com/fluidprop/`.

[8] P. Colonna, E. Casati, C. Trapp, T. Mathijssen, J. Larjola, T. Turunen-Saaresti, and A. Uusitalo. Organic Rankine Cycle Power Systems: From the Concept to Current Technology, Applications, and an Outlook to the Future. *Journal of Engineering for Gas Turbines and Power*, 137, 10 2015. doi: 10.1115/1.4029884.

[9] Dallara, E. Schwartz, K. I. M, and W. I. A. Metric for Comparing Lifetime Average Climate Impact of Aircraft. *AIAA journal*, 49(8):1600–1613, 2011.

[10] R. De Vries, M. Brown, and R. Vos. A Preliminary Sizing Method for Hybrid-Electric Aircraft Including Aero-Propulsive Interaction Effects. Atlanta, Georgia, USA, 2018. AIAA Aviation Forum. doi: 10.2514/6.2018-4228.

[11] S. Defoort, E. Nguyen, and P. Schmollgruber. Personal Communication with ONERA, 2023.

[12] ESDU. ESDU86002: Drag and Pressure Recovery Characteristics of Auxiliary Air Inlets at Subsonic Speeds, 2004.

[13] J. W. Gauntner. Algorithm for Calculating Turbine Cooling Flow and the Resulting Decrease in Turbine Efficiency. Technical report, NASA Lewis Research Centre, 1980. NASA-TM-81453.

[14] H. Gesell, F. Wolters, and M. Plohr. System Analysis of Turbo-electric and Hybrid-electric Propulsion Systems on a Regional Aircraft. *The Aeronautical Journal*, 123(1268):1602â1617, 2019. doi: 10.1017/aer.2019.61.

[15] A. Giuffré and M. Pini. Design Guidelines for Axial Turbines Operating with Non-ideal Compressible Flows. *Journal of Engineering for Gas Turbines and Power*, 143(1):011004, 2021. doi: 10.1115/1.4049137.

[16] J. S. Gray, J. T. Hwang, J. R. R. A. Martins, K. T. Moore, and B. A. Naylor. OpenMDAO: An open-source framework for multidisciplinary design, analysis, and optimization. *Structural and Multidisciplinary Optimization*, 59 (4):1075–1104, April 2019. doi: 10.1007/s00158-019-02211-z.

[17] GRETh. Echtherm. URL `https://greth.fr/echtherm/`. version 3.2.

[18] H. Grieb. *Projektierung von Turboflugtriebwerken*. BirkhÃ¤user Basel, 2004. doi: 10.1007/978-3-0348-7938-5.

[19] E. S. Hendricks and J. S. Gray. pyCycle: A Tool for Efficient Optimization of Gas Turbine Engine Cycles. *Aerospace 2019, Vol. 6, Page 87*, 6:87, 8 2019. doi: 10.3390/AEROSPACE6080087.

[20] M. Hughes and J. Olsen. Fuel Burn Reduction of Hybrid Aircraft Employing an Exhaust Heat Harvesting System. *Journal of Propulsion and Power*, 38:241–253, 9 2022. doi: 10.2514/1.B38393.

[21] B. P. James and B. Zahawi. High Speed Generator for Turbocharger Based Domestic Combined Heat and Power Unit Employing the Inverted Brayton Cycle. *Energy Procedia*, 42:249–260, 2013. doi: https://doi.org/10.1016/j.egypro.2013.11.025.

[22] Jane's Information Group. Jane's aero-engines, 2022.

[23] D. Japikse. *Centrifugal Compressor Design and Performance*. Concepts ETI, 1996.

[24] S. M. Jones, W. J. Haller, and M. T.-H. Tong. An N+3 Technology Level Reference Propulsion System. Technical report, NASA Glenn Research Centre, 2017. NASA/TM-2017-219501.

[25] Kaltra GmbH. Microchannel Condensers: Heat Exchangers for Condenser Applications. Technical report, 2020. URL `https://www.kaltra.com/wp-content/uploads/2020/04/TM_Microchannel-Condensers_Ver.3.0_EN.pdf`. Accessed on 16 June 2023.

[26] K. Kawagishi, A. C. Yeh, T. Yokokawa, T. Kobayashi, Y. Koizumi, and H. Harada. Development of an Oxidation-resistant High-strength Sixth-Generation Single-crystal Superalloy TMS-238. *Superalloys 2012*, pages 189–195, 10 2012. doi: 10.1002/9781118516430.CH21.

[27] Knowledge Center on Organic Rankine Cycle technology. Thermal Energy Harvesting The Path to Tapping into a Large CO_2-free European Power Source, 2022. URL `https://kcorc.org/en/committees/thermal-energy-harvesting-advocacy-group/`.

[28] D. Krempus, S. Bahamonde, T. V. D. Stelt, C. M. D. Servi, W. Klink, and P. Colonna. On Mixtures as Working Fluids for Air-cooled ORC Bottoming Power Plants of Gas Turbines. online, 2021. 6th International Seminar on ORC Power Systems.

[29] D. Krempus, F. Beltrame, M. Majer, C. M. D. Servi, M. Pini, R. Vos, and P. Colonna. Organic Rankine Cycle Waste Heat Recovery Systems for Aircraft Auxiliary Power Units. Toulouse, France, 2022. Towards Sustainable Aviation Summit.

[30] H. D. Kwak, S. Kwon, and C. H. Choi. Performance Assessment of Electrically Driven Pump-fed LOX/Kerosene Cycle Rocket Engine: Comparison with Gas Generator Cycle. *Aerospace Science and Technology*, 77:67–82, 6 2018. doi: 10.1016/J.AST.2018.02.033.

[31] K. Kyprianidis. *On Gas Turbine Conceptual Design*. Phd thesis, Cranfield University, 2019.

[32] D. Lee, D. Fahey, A. Skowron, M. Allen, U. Burkhardt, Q. Chen, S. Doherty, S. Freeman, P. Forster, J. Fuglestvedt, A. Gettelman, R. De León, L. Lim, M. Lund, R. Millar, B. Owen, J. Penner, G. Pitari, M. Prather, R. Sausen, and L. Wilcox. The Contribution of Global Aviation to Anthropogenic Climate Forcing for 2000 to 2018. *Atmospheric Environment*, 244:117834, 2021. doi: https://doi.org/10.1016/j.atmosenv.2020.117834.

[33] E. W. Lemmon, I. H. Bell, M. L. Huber, and M. O. McLinden. NIST Standard Reference Database 23: Reference Fluid Thermodynamic and Transport Properties-REFPROP, Version 10.0, National Institute of Standards and Technology, 2018.

[34] J. D. Mattingly, W. H. Heiser, K. M. Boyer, B. A. Haven, and D. T. Pratt. *Aircraft Engine Design*. AIAA, 3rd edition, 2018.

[35] M. R. Nichols. Investigation of Flow Through an Intercooler Set at Various Angles to the Supply Duct. Technical report, NASA Langley Research Center, 1942. Technical Report.

[36] E. Obert. *Aerodynamic Design of Transport Aircraft*. IOS Press, 2009.

[37] C. A. Perullo, D. N. Mavris, and E. Fonseca. An Integrated Assessment of an Organic Rankine Cycle Concept for Use in Onboard Aircraft Power Generation. volume 2, San Antonio, Texas, USA, 2013. Proceedings of the ASME Turbo Expo. doi: 10.1115/GT2013-95734.

[38] R. Pouzolz, O. Schmitz, and H. Klingels. Evaluation of the Climate Impact Reduction Potential of the Water-Enhanced Turbofan (WET) Concept. *Aerospace*, 8(3), 2021. doi: 10.3390/aerospace8030059.

[39] M. Ridel, E. Nguyen Van, T. Prosvirnova, D. Donjat, C. Seguin, and P. Choy. DRAGON: hybrid electrical architecture for distributed fans propulsion. Bordeaux, France, 2021. MEA.

[40] S. Samuelsson, T. Gronstedt, and K. G. Kyprianidis. Consistent Conceptual Design and Performance Modeling of Aero Engines. *Proceedings of the ASME Turbo Expo*, 3, 8 2015. doi: 10.1115/GT2015-43331.

[41] H. I. H. Saravanamuttoo, G. F. C. Rogers, H. Cohen, P. V. Straznicky, and A. C. Nix. *Gas Turbine Theory*. Pearson Education, 7th edition, 2017. ISBN 0132224372.

[42] J. W. Sawyer. *Sawyer's Gas Turbine Engineering Handbook, Volume 1: Theory & Design*. Turbomachinery International Publications, 3rd edition, 1985. ISBN 0-937506-14-1.

[43] P. Schmollgruber, D. Donjat, M. Ridel, I. Cafarelli, O. Atinault, C. F. cois, and B. Paluch. Multidisciplinary Design and Performance of the ONERA Hybrid Electric Distributed Propulsion Concept (Dragon). pages 1–27, online, 2020. AIAA Scitech Forum 2020. doi: 10.2514/6.2020-0501.

[44] G. Sovran and E. D.Klomp. Experimentally Determined Optimum Geometries for Rectilinear Diffusers with Rectangular, Conical or Annular Cross-section. Technical report, General Motors Research Laboratories, 1968.

[45] E. Torenbeek. *Synthesis of Subsonic Airplane Design*. Delft University Press, 1982.

[46] E. Torenbeek. The Initial Calculation of Range and Mission Fuel During Conceptual Design. *Delft University of Technology, Faculty of Aerospace Engineering, Report LR-525*, 1987.

[47] E. Torenbeek. *Advanced Aircraft Design*. John Wiley and Sons, 2013.

[48] M. van der Geest, H. Polinder, J. A. Ferreira, and M. Christmann. Power Density Limits and Design Trends of High-Speed Permanent Magnet Synchronous Machines. *IEEE Transactions on Transportation Electrification*, 1 (3):266–276, 2015. doi: 10.1109/TTE.2015.2475751.

[49] L. Xu, K. G. Kyprianidis, and T. U. Grönstedt. Optimization Study of an Intercooled Recuperated Aero-engine. *Journal of Propulsion and Power*, 29:424–432, 2013. doi: 10.2514/1.B34594.

[50] K. Zarati, S. Maalouf, and A. T. Isikveren. Potential of the Bottom Organic Rankine Cycle to Recover Energy on Turboprop Engine Architecture. Manchester, UK, 2017. 23rd ISABE Conference.